Nanoscale

PAPER

View Article Online
View Journal | View Issue

Cite this: *Nanoscale*, 2018, **10**, 10116

The owl sensor: a 'fragile' DNA nanostructure for the analysis of single nucleotide variations†

Rebekah J. Karadeema,*‡[a] Maria Stancescu,[a] Tyler P. Steidl,[a,b] Sophia C. Bertot[a,b] and Dmitry M. Kolpashchikov *[a,b,c,d]

Received 7th February 2018,
Accepted 26th April 2018

DOI: 10.1039/c8nr01107a

rsc.li/nanoscale

Analysis of single nucleotide variations (SNVs) in DNA and RNA sequences is instrumental in healthcare for the detection of genetic and infectious diseases and drug-resistant pathogens. Here we took advantage of the developments in DNA nanotechnology to design a hybridization sensor, named the 'owl sensor', which produces a fluorescence signal only when it complexes with fully complementary DNA or RNA analytes. The novelty of the owl sensor operation is that the selectivity of analyte recognition is, at least in part, determined by the structural rigidity and stability of the entire DNA nanostructure rather than exclusively by the stability of the analyte–probe duplex, as is the case for conventional hybridization probes. Using two DNA and two RNA analytes we demonstrated that owl sensors differentiate SNVs in a wide temperature range of 5 °C–32 °C, a performance unachievable by conventional hybridization probes including the molecular beacon probe. The owl sensor reliably detects cognate analytes even in the presence of 100 times excess of single base mismatched sequences. The approach, therefore, promises to add to the toolbox for the diagnosis of SNVs at ambient temperatures.

The diagnosis and appropriate treatment of human genetic disorders and infectious diseases rely on the analysis of single nucleotide (nt) variations (SNVs), which include substitutions, insertions, and deletions.[1] Hybridization probes traditionally used for SNV analysis bind a fragment of DNA or RNA containing an SNV site and form a complex, which has greater stability if fully complementary, *i.e.* all Watson–Crick base pairs are formed between the probe and the analyte, than if a single mispairing is present.[2] Upon subjection of the complex to increasing temperatures the fully matched hybrid decomposes (melts) at higher temperatures than the mismatched complex.[3] This technique enables differentiation of SNVs at high temperatures (>40 °C), but only over narrow temperature ranges. The variations of hybridization probes developed so far include peptide nucleic acids (PNAs),[4] locked nucleic acids (LNAs),[5] molecular beacon (MB) probes,[6] and binary probes.[7] All probes rely on this same idea for SNV analysis: the difference in the Gibbs energies between matched and mismatched complexes, which has constant and limited value.[8] For example, if the probe binds a 10-nt segment (which is close to the shortest possible in practice), a single base mispairing will destabilize the complex by only ~10% on average. While increasing the length of the recognized fragment provides greater affinity and sensitivity, a mispairing then contributes to a proportionally lower destabilization effect, leading to even poorer differentiation. Balancing probe affinity and selectivity is a fundamental limitation of the conventional hybridization probes.[8] Therefore, despite many years of effort, SNV analysis *via* hybridization probes remains challenging, especially at temperatures below 40 °C.[7–9] On the other hand, enzymes recognize SNVs at ambient temperatures, presumably due to their more sophisticated recognition strategy.[10] We hypothesized that enzyme-free DNA probes that, along with the base pairing, use additional principles of target recognition would enable high selectivity of SNV recognition even at ambient temperatures. One implementation of this idea is multicomponent X sensors (see below),[11] which differentiate mismatches at ambient temperature.

In this work, we were inspired by the engineering concept that recognizes that a small and localized failure in an 'imperfectly' designed system is likely to result in a structure's collapse. For example, a stable bridge, but not the one with a

[a]*Chemistry Department, University of Central Florida, Orlando, FL 32816, USA. E-mail: rebekah@scripps.edu, dmitry.kolpashchikov@ucf.edu*
[b]*Burnett School of Biomedical Sciences, University of Central Florida, Orlando, 32816 Florida, USA*
[c]*National Center for Forensic Science and Burnett School of Biomedical Sciences, University of Central Florida, Orlando, Florida, 32816, USA*
[d]*ITMO University, Laboratory of Solution Chemistry of Advanced Materials and Technologies, Lomonosova St. 9, 191002 St Petersburg, Russian Federation*

†Electronic supplementary information (ESI) available: Details of experimental procedures, list of all DNA and RNA sequences used in this study as well as the experimental data supporting the conclusions made in this study. See DOI: 10.1039/c8nr01107a

‡Current address: Department of Chemistry, The Scripps Research Institute, 10550 North Torrey Pines Road, La Jolla, California 92037, USA.

structural defect, can absorb stress on its support system.[12] Keeping in mind that a rigid object fails more easily than a ductile/flexible one,[13] we took advantage of DNA nanotechnology[14] and designed a DNA sensor that forms a rigid and structurally imperfect complex when it binds to a complementary analyte. A single base mismatch serves the role of 'stress' and causes the collapse of the entire fluorescent structure, allowing the sensor to effectively differentiate between fully complementary and mismatched analytes.

The owl sensor consists of two DNA adaptor strands R_x and P_y and a universal molecular beacon (UMB) probe. The UMB probe does not directly bind the analyte and therefore can be used for analysis of any sequence given that the adaptor strands are adjusted accondingly.[15] The central portions of the adaptor strands are complementary to the analyte and are thus called analyte-binding domains, while the 4- to 5-nt long 3′ and 5′ terminal sequences are complementary to the UMB. The adaptor strands are named R_x and P_y (Fig. 1a), where x and y stand for the number of nts in the analyte-binding domains. In the presence of a specific analyte, R_x and P_y bind to both UMB and the analyte thus forming a 4-stranded fluorescent structure, which, when drawn, resembles owl eyes, suggesting the name of the structure and the sensor. The structure contains a DNA 4-way junction (crossover) motif commonly used in DNA and RNA nanotechnology.[16]

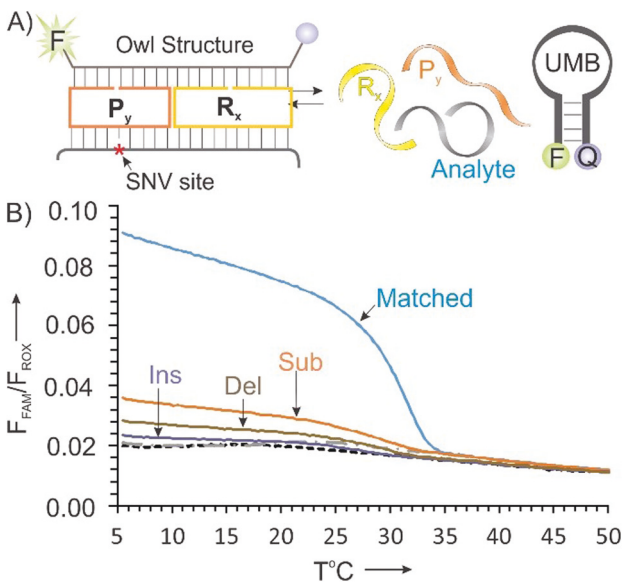

Fig. 1 Design and performance of the owl sensor. (A) The adaptor strands R_x and P_y reversibly hybridize to the analyte and the universal molecular beacon (UMB) probe, forming a fluorescent owl structure (see Fig. S1† for more details). (B) Melting curves for R_{10}/P_9 owl sensor (**R_{10}**: 5′-TAT TGA GTG GCC CAT CGA TC, P_9: 5′- TAA CTG TTG TGT CTA TGT; and **UMB1**, 5′-/FAM/-CGC GTT AAC ATA CAA TAG ATC GCG-/BHQ1/) in the presence of fully matched **InhC** (5′-GCG GCA TGG GTA TGG GCC ACT GAC ACA ACA CAA GGA C) or SNV-containing analytes: substitution (Sub), deletion (Del) or insertion (Ins) (see Table S1† for full sequences). Grey dotted-dashed line: no analyte control; black dashed line: **UMB1** only. The samples contained 50 mM Tris-HCl, pH 7.4, 50 mM $MgCl_2$, and 0.1% Tween-20 with 50 nM **UMB1**, 50 nM ROX, 150 nM **R_{10}**, 200 nM **P_9**, and 100 nM analytes. The ROX dye was used as an internal control for normalization of fluorescence from different samples (see the ESI† for details). The experimental data are averages of 3 experiments.

As a model analyte, we used a fragment of a gene which codes for enoyl-acyl carrier protein reductase (inhA), a target for the antibiotic isoniazid, which is a common treatment for *Mycobacterium tuberculosis (Mtb)* infection.[17] SNVs in this gene are known to impart Mtb resistance to isoniazid.[17] The analyte named **InhC** was fully matched to the sensor, while **InhT** contained a G-T mispairing, which is known to be the least destabilizing and, therefore, the most challenging mismatch to detect in DNA.[18] We also designed an analyte with a one-nucleotide deletion, **Inh_del**, and an analyte with a one-nucleotide insertion, **Inh_ins** (Table S1†), mutations not seen in *Mtb*, but allowing for the versatility of the sensor to be demonstrated. The analytes folded in a relatively unstable secondary structure under the assay conditions (Fig. S1†). The sequence of the **UMB1** probe (see Fig. 1 legend) was optimized by us earlier.[15] In this study, we demonstrate that the owl sensor enables differentiation of fully matched analytes from SNV-containing analytes in a broad temperature range that includes ambient temperatures. Furthermore, we aimed to show that this property, at least in part, can be attributed to the rigidity of the owl structure.

The owl structure is more rigid than dsDNA formed in the case of conventional probes because (i) DNA crossover tiles (even with free ends) are known to be more rigid than dsDNA;[16] and (ii) the ends of the P and R strands are fixed, both by hybridization to **UMB1** and by stacking interactions of both 3′ and 5′ terminal base pairs in each strand. To the best of our knowledge, this last feature is absent in the designs of all other hybridization probes, where the location of the ends of the probe is independent of the DNA helical path. Therefore, the length of the analyte-binding fragment of R_x and P_y should correspond to a full helical turn of B DNA (~10 nts) to provide the greatest stability to the owl structure.

Indeed, when different lengths of **R_x** with **P_{10}** were tested, we found that R_{10}/P_{10} produced the highest melting temperature, an indication of complex stability (compare Fig. 1 with S2†). However, as expected, the stable R_{10}/P_{10} complex was able to tolerate an SNV and thus produced nearly the same signal in the presence of the mismatched **InhT** as with the fully matched **InhC** (Fig. S2C†). This proves our hypothesis that 'perfectly' designed DNA nanostructures (the owl complex formed by R_{10} and P_{10}) are able to tolerate stress in the form of base mispairing. For the owl sensor to collapse in the presence of a mismatch, 'imperfect' designs were explored, in which the lengths of analyte-binding fragments were changed from a perfect 10 to imperfect 12, 11, 9 or 8 nts (Fig. 1, S2, and S3†). We found that **R_{10}/P_9** allows for complex formation from 5 to about 34 °C with the correct analyte, while SNV-containing analytes resulted in little or no signal above the background in this temperature interval (Fig. 1B). This result supports our assumption that the R_{10}/P_9 owl sensor cannot withstand additional stress introduced by the SNVs due to the strain in

structure induced by the 'imperfect helicity' (Fig. 1a). R_{10}/P_8 produced no signal above the background in the presence of either analyte (Fig. S3†) due to the insufficient stability of the owl structure.

We then compared the SNV differentiation ability of the R_{10}/P_9 sensor with linear and MB probes and X sensor, which were designed to differentiate the SNVs according to the previously developed stretagies[5,6,11] (Fig. 2A). Fig. 2B demonstrates the ratios of fluorescent signals in the presence of fully matched **InhC** to that of the single base mismatched **InhT**. We assumed that the SNV was differentiated if the signal of the matched analyte (F_m) divided by that of the mismatched analyte (F_{mm}) was greater than 1.5, a parameter named $\Delta T_{1.5}$.[11d] Based on this criterion, the R_{10}/P_9 owl sensor differentiated the SNV between 5 and 32.4 °C ($\Delta T_{1.5}$ = 27.4 °C), an interval significantly greater than that for the linear probe ($\Delta T_{1.5}$ = 14.8 °C), MB probe ($\Delta T_{1.5}$ = 15.6 °C), and X sensor ($\Delta T_{1.5}$ = 17.9 °C). Similar results were obtained for the deletion- and insertion-containing analytes (Fig. S5†), as well as for the R_{10}/P_9 Owl Sensor specific to the **InhT** analyte (Fig. S6†). Importantly, the linear and MB probes differentiated analytes at temperatures above physiological values (>45 °C Fig. 2B), which is common for conventional probes.[5,6] Therefore, the owl sensor has two practical advantages over the traditional hybridization probes: it enables (i) broadening the temperature differentiation range, and (ii) shifting its differentiation interval to lower (ambient) temperatures. The limit of detection (LOD) of the owl sensor was found to be 4.9 nM, which was not significantly affected by the presence of 100 times excess of the single base mismatched analyte (Fig. S7†). This LOD is comparable with that of MB probes.[6b]

The remarkably improved SNV differentiation ability of R_{10}/P_9 in comparison with the R_{10}/P_{10} sensor could be explained by both the reduced stability of the analyte–P9 in comparison with the analyte–P10 complex, as is the case for the conventional probes. Alternatively, the instability of the owl structure as a whole due to the 'imperfect' design could be the main contributor to its differentiation ability. If the latter is true, addition of structural flexibility to the owl structure should jeopardize this extraordinary SNV differentiation ability.

To test this hypothesis, we added flexible triethylene glycol (TEG) linkers between the analyte- and MB-binding arms at the strand crossover points (Fig. 3A). PEG linkers connecting two DNA fragments are known to increase the flexibility of DNA constructs.[19] The owl strands containing linkers had the following labels: outside junction (o-TEG), inside junction (i-TEG), or to both junctions (TEG_D) (Fig. 3A). TEG-containing owl sensors were subjected to the melt curve procedure to

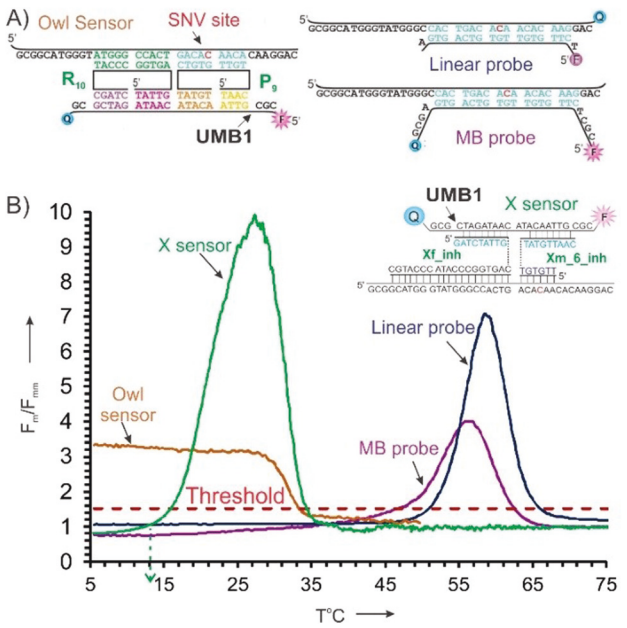

Fig. 2 SNV differentiation by various hybridization probes. (A) owl sensor R_{10}/P_9, linear probe, MB probe, and the X sensor in complex with analytes **inhC/inhC_Q**. The red 'C' indicates the location of the SNV site. (B) Differentiation ability (F_m/F_{mm}) of the linear probe (blue line), the MB probe (purple line), X sensor (magenta line) and the owl sensor (green line) as a function of temperature. F_m/F_{mm} is defined as a ratio of fluorescence intensities produced by each probe in the presence of fully matched analyte (F_m) **InhC** to that of mismatched **InhT** analyte (F_{mm}) after subtraction of the background. The **InhT** analyte contained a C > T substitution with respect to the **InhC** analyte. Unless otherwise specified, the P strand of the owl sensor was specific to the **InhC** version of the analyte. The threshold of the F_m/F_{mm} ~ 1.5 is indicated by the red dotted line. The original fluorescence data used for the plot are shown in Fig. 1B and S4.† The experimental data are averages of 3 experiments.

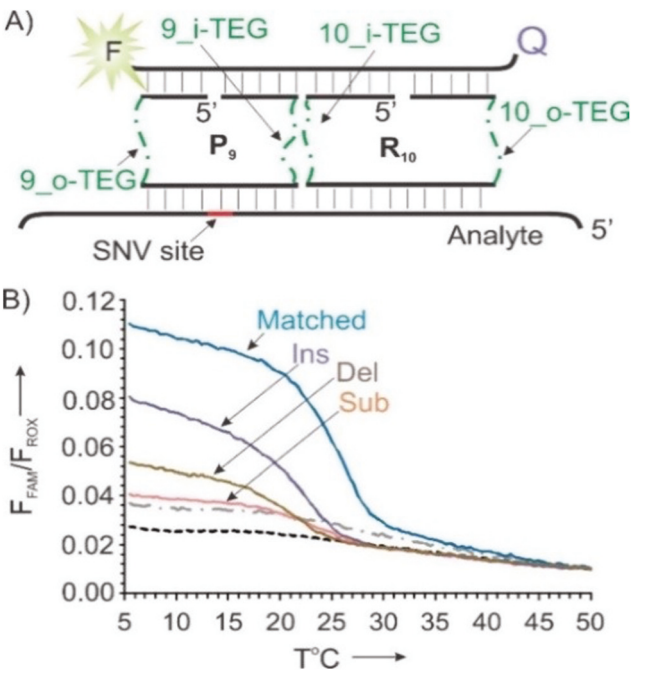

Fig. 3 Introduction of flexible triethylene glycol (TEG) linkers reduced the SNV-differentiation ability of owl sensors. (A) Location of TEG linkers in the owl structure (green). (B) Fluorescence response of the $R_{10\text{-oTEG}}/P_9$ sensor in the presence of matched InhC, or SNV-containing **Inh_T**, **Inh_ins** and **Inh_del**. Grey dotted-dashed line: no analyte control; black dashed line: **UMB1** only. The experimental conditions were as described in Fig. 1B legend. The experimental data are averages of 3 experiments.

determine the effect of their flexibility on T_m and $\Delta T_{1.5}$. Overall, the SNV differentiation ability of the TEG-containing sensors was significantly reduced: $\Delta T_{1.5}$ dropped from 27.4 °C from the R_{10}/P_9 sensor to as low as 0 for some PEGylated constructs (Table 1). A single TEG linker in the R_{10} strand resulted in poor differentiation of insertion (Ins) and deletion (Del) SNVs (Fig. 3B) in comparison with the linker-free R_{10}/P_9 (Fig. 1B). This result suggests that the rigidity of the entire owl structure (not only the length of the $\mathbf{P_9}$–analyte complex) is important for SNV differentiation. It is interesting to note that, when TEG-containing strands were used, a significant signal with the **Inh_ins** analyte was observed, indicating that a flexible system tends to accommodate an extra nucleotide in the analyte strand (Fig. S8–10†).

Earlier we demonstrated the ability of the X sensor to differentiate the SNV containing analytes in the temperature range of 5–40 °C due to the multistage recognition of the target with the limiting stage requiring the same activation energy for matched and mismatched analytes, which leads to the effect termed 'kinetic inversion'.[11d] It has been well established that a linear or MB probe equilibrates with a mismatched analyte faster than with fully matched analytes.[11d,20] Thus achieving equilibrium conditions was considered essential to achieve the best SNV differentiation. The 'kinetic inversion' effect enables the opposite: faster equilibration of a complex with fully matched nucleic acids, which results in excellent SNV differentiation earlier in the hybridization reaction. For hybridization of the X sensor, we observed the 'kinetic inversion' effect in this study. Indeed, the fluorescence of the X sensor in the presence of **Inh_C** achieved a plateau given ~200 s for equilibration, while a longer time of ~600 s was required for equilibration with mismatched **Inh_T** (Fig. 4, orange lines). It should be noted, that with Inh analytes the 'kinetic inversion' effect was less pronounced than with analytes used previously,[11d] presumably due to the difference in the stability of analyte secondary structures (a detailed investigation of this difference is in progress). However, we did not observe the 'kinetic inversion' effect for the owl sensor: the reaction mixture with mismatched **Inh_T** reached a plateau faster (in about 600 s) than fully matched **Inh_C** (no signal stabilization even after 1800 s; Fig. 4, green lines). We conclude, therefore, that the owl sensor utilizes a different SNV differentiation strategy than the X sensor, a phenomenon that may become practically important. Indeed, the X sensor, designed according to the previously established rules, failed to differentiate **Inh_C** from **Inh_T** at temperatures below 15 °C (Fig. 2B and S11†). Therefore, if a differentiation of SNVs in analytes with unstable secondary structures needs to be achieved at temperatures below 15 °C, the owl sensor design should be utilized.

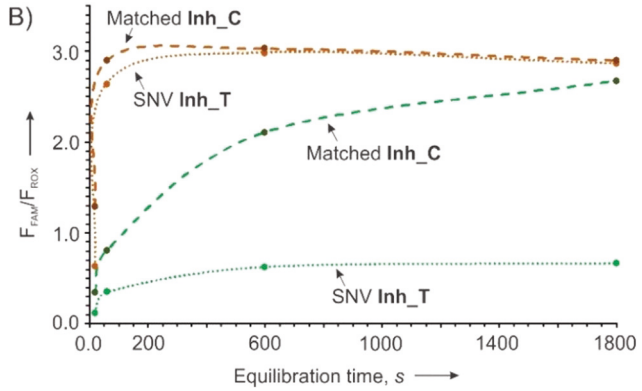

Fig. 4 Florescence of probe–analyte complexes at different rates of the cooling–heating cycle. The fluorescence signal for the equilibration time periods of 20, 60, 600 or 1800 s/1 °C observed for the X sensor-analyte (orange lines) and $\mathbf{R_{10}/P_9}$ Owl Sensor (green lines) at 10 °C. In the presence of a fully matched **Inh_C** (dashed lines) or single base mismatched **Inh_T** (dotted lines). The experimental data are averages of 3 experiments.

Further we explored the ability of the owl sensor to analyze RNA sequences. RNA–DNA hybrids typically adopt an A DNA-like conformation with 11.1 bp per helical turn (not 10.4 bp per turn as it is for B DNA). We investigated the performance of a series of owl sensors with the RNA analogs of **InhC** and **InhT** analytes (Fig. S12 and S13†). It was found that R_{11}/P_9 performed best (differentiation from 5 to 25.1 °C), while R_{10}/P_9 failed to produce a significant signal. This proves that optimum helicity in the R strand is needed for sensing. The owl sensor, therefore, is applicable for highly selective analysis of RNA sequences with a slight change in the adapter strand used for analysis of DNA sequences.

To prove the general applicability of the owl sensor design, we used another pair of arbitrarily chosen analytes: miRNA99a and miRNA100, which differ by a single nt (TableS1, Fig. S14 and 15†). Altered expression of these miRNAs has been found in various cancers, including breast cancer.[21] Owl sensors specific to both RNA and DNA (miDNA99a and miDNA100) versions of the target were designed and tested. As is the case with Inh-related analytes, R_{10mi} was the best for DNA analytes while R_{11mi} performed best for RNA analytes (Fig. S16 and 17†). We also observed high selectivity of SNV recognition

Table 1 Quantitative assessment of the stability (T_m) and differentiation ability ($\Delta T_{1.5}$) of the R_{10}/P_9 owl sensor with and without TEG linkers

DNA strand combinations[a]		T_m, °C Matched	$\Delta T_{1.5}$, °C		
R	**P**		**InhT**	**Inh-Del**	**Inh-Ins**
10	**9**	31.6	27.6	27.9	27.6
10	**9_A**	31.5	27.8	27.9	27.8
10	**9_o-TEG**	31.3	28.0	28.3	27.6
10	**9_i-TEG**	23.9	20.0	20.8	0.0
10	**9_TEG_D**	23.7	0.0	0.0	0.0
10_o-TEG	**9**	26.2	23.1	23.4	11.9
10_TEG_D	**9**	15.6	8.2	10.5	0.0
10_i-TEG	**9**	19.0	12.4	13.6	0.0
10_o-TEG	**9_o-TEG**	25.5	18.2	19.9	0.0
10_i-TEG	**9_i-TEG**	27.8	24.0	24.0	0.0
10_TEG_D	**9_TEG_D**	23.8	19.4	19.4	18.2

[a] T_m is the melting temperature determined from the data presented in Fig. 1B, 2B, S6, S8, S9, and S10; $\Delta T_{1.5}$ (see the explanation in the Fig. 2 legend).

under ambient temperatures (Fig. S17†). The corresponding **miRNA100** was differentiated with high selectivity from **miRNA99a** using an $\mathbf{R_{11\_mi}/P_{9\_mi\_100}}$ sensor (Fig. 5), but not sensors with $\mathbf{R_{10\_mi}}$ or $\mathbf{R_{12\_mi}}$ strands (Fig. S18 and 19†). These results suggest the general applicability of the owl sensor design for analysis of potentially any DNA or RNA sequence. We also investigated the sensor's performance in the presence of excess unrelated biological RNA. It was found that the presence of 2.5 mg L^{-1} or 25 mg L^{-1} yeast RNA does not significantly affect the performance of the owl sensor (Fig. S20†). This data further highlights the high selectivity of the developed approach as well as robustness of the owl sensor's performance in the presence of bulk amounts of biological molecules.

Traditional design of the SNV-specific hybridization probes is time-consuming. Even if perfectly designed and under optimal hybridization conditions, such sensors have limited SNV selectivity, especially at practically important ambient temperatures. Here we applied of a new concept of analyte recognition, in which a hybridization sensor uses an analyte as a scaffold to build a rigid and fragile nanostructure that is too unstable if an SNV is present. The design procedure is as follows: (i) always use **UMB1** (5′-/FAM/-CGC GTT AAC ATA CAA TAG ATC GCG-/BHQ1/) as a fluorescent reporter; (ii) always use UMB1-binding arms for strands P and R as shown in Fig. 2 and 5 for DNA and RNA analytes, respectively; (iii) the SNP site should be located in the middle position of the P strand-binding region; (iv) the analyte binding arm of strand R should hybridize adjacent to the hybridization site of strand P and should be 10 and 11 nucleotides for the analyses of DNA and RNA analytes, respectively. Therefore, unlike conventional hybridization-based sensors, this design promises to eliminate the need for adjusting the probe lengths or the hybridization conditions to achieve near-perfect selectivity. The new sensor selectively binds only to fully complementary DNA and RNA and discriminates against single base substitutions, deletions, and insertions in a broad temperature range even in the presence of random RNA or excess amount of single base-mismatched analyte. For two different analyte sequences, it was shown that 10 and 9 nts for the R and P strands, respectively, were ideal for DNA-targeting sensors, while 11 and 9 nts for the R and P strands, respectively, worked best for RNA targeting. Follow up studies are in progress for further verification of the general applicability of the owl sensor for DNA and RNA analysis. Importantly, the **UMB1** does not hybridize directly to the analyte in the owl complex and, therefore, can be used universally for any analyte, provided that strands P and R are tailored for targeted sequences. The owl sensor, therefore, promises to simplify the design and optimization of hybridization assays and will contribute to low cost, ambient temperature analysis of DNA and RNA.

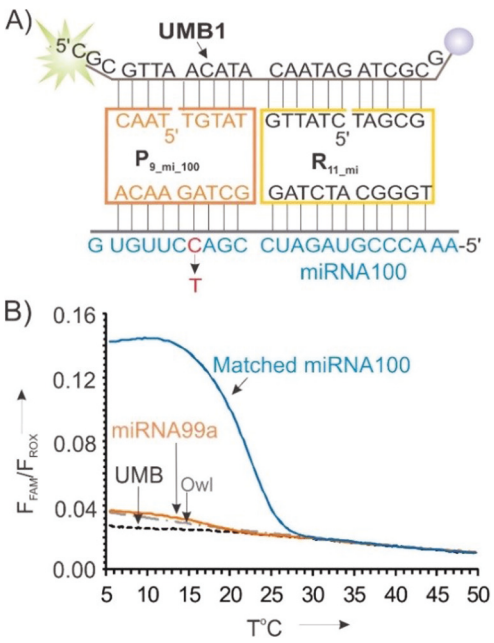

Fig. 5 $\mathbf{R_{11}/P_9}$ owl sensor differentiates single base mismatch in RNA analytes. (A) $\mathbf{R_{11\_mi}/P_{9\_mi\_100}}$ sensor in a complex with fully matched **miRNA100**. The red letter indicates the SNV position. (B) Melting curves for $\mathbf{R_{11\_mi}/P_{9\_mi\_100}}$ complexes with matched **miRNA100** (blue) and single base mismatched **miRNA99a** (orange) analytes. The samples contained 50 mM Tris-HCl, pH 7.4, 10 mM $MgCl_2$, and 0.1% Tween-20 with 50 nM **UMB1**, 50 nM ROX, 150 nM $\mathbf{R_{11\_mi}}$, 200 nM $\mathbf{P_{9\_mi\_100}}$, and 100 nM analytes. The ROX dye was used as an internal control for the normalization of fluorescence from different samples (see the ESI† for details). The experimental data are averages of 3 experiments.

Author contributions

R. J. K., M. S., and D. M. K. conceived the experiments. R. J. K., M. S., T. P. S., and S. C. B. carried out the experiments. R. J. K. and D. M. K. wrote the manuscript with support from M. S., T. P. S., and S. C. B. All authors provided critical feedback and helped shape the research, analysis and manuscript.

Funding sources

This project was supported by the NSF CCF 1423219 and NSF CBET 1706802. D. M. K. was supported by the ITMO University Fellowship and Professorship Program.

Abbreviations

UMB	Universal molecular beacon
nt	Nucleotide
SNV	Single nucleotide variation
MB	Molecular beacon
PNAs	Peptide nucleic acids
LNAs	Locked nucleic acids
Mtb	*Mycobacterium tuberculosis*
LOD	Limit of detection
F_m	Fluorescence of matched analyte
F_{mm}	Fluorescence of mismatched analyte
T_m	Melting temperature
TEG	Triethylene glycol

Conflicts of interest

There are no conflicts to declare.

Acknowledgements

DMK is grateful to Dr Yulia V. Gerasimova for helpful discussion and help with manuscript preparation.

References

1 (*a*) I. Aphasizheva and R. Aphasizhev, *Trends Parasitol.*, 2016, **32**, 144–156; (*b*) K. D. Makova and R. C. Hardison, *Nat. Rev. Genet.*, 2015, **16**, 213–323; (*c*) C. Yu, B. T. Baune, J. Licinio and M. L. Wong, *Psychiatry Res.*, 2017, **252**, 75–79.

2 (*a*) S. A. Marras, S. Tyagi and F. R. Kramer, *Clin. Chim. Acta*, 2006, **363**, 48–60; (*b*) A. S. Boutorine, D. S. Novopashina, O. A. Krasheninina, K. Nozeret and A. G. Venyaminova, *Molecules*, 2013, **18**, 15357–15397; (*c*) J. Guo, J. Ju and N. Turro, *Anal. Bioanal. Chem.*, 2012, **402**, 3115; (*d*) N. P. Junager, J. Kongsted and K. Astakhova, *Sensors*, 2016, **16**, pii: E1173.

3 (*a*) M. Erali, K. V. Voelkerding and C. T. Wittwer, *Exp. Mol. Pathol.*, 2008, **85**, 50–58; (*b*) S. Fontenete, N. Guimarães, J. Wengel and N. F. Azevedo, *Crit. Rev. Biotechnol.*, 2016, **36**, 566–577; (*c*) S. Y. Tong and P. M. Giffard, *J. Clin. Microbiol.*, 2012, **50**, 3418–3421.

4 (*a*) N. Zhang and D. H. Appella, *J. Infect. Dis.*, 2010, **201**, S42–S45; (*b*) Q. Liu, J. Wang and B. J. Boyd, *Talanta*, 2015, **136**, 114–127; (*c*) J. Lee, I. S. Park, E. Jung, Y. Lee and D. H. Min, *Biosens. Bioelectron.*, 2014, **62**, 140–144; (*d*) I. V. Smolina and M. D. Frank-Kamenetskii, *Methods Mol. Biol.*, 2014, **1050**, 121–130; (*e*) C. Sharma and S. K. Awasthi, *Chem. Biol. Drug Des.*, 2017, **89**, 16–37.

5 (*a*) M. A. Campbell and J. Wengel, *Chem. Soc. Rev.*, 2011, **40**, 5680–5689; (*b*) D. Xi, J. Shang, E. Fan, J. You, S. Zhang and H. Wang, *Anal. Chem.*, 2016, **88**, 10540–10546; (*c*) S. Fontenete, D. Carvalho, N. Guimarães, P. Madureira, C. Figueiredo, J. Wengel and N. F. Azevedo, *Appl. Microbiol. Biotechnol.*, 2016, **100**, 5897–5906.

6 (*a*) S. Tyagi and F. R. Kramer, *Nat. Biotechnol.*, 1996, **14**, 303–308; (*b*) D. M. Kolpashchikov, *Scientifica*, 2012, 928783.

7 D. M. Kolpashchikov, *Chem. Rev.*, 2010, **110**, 4709–4723.

8 (*a*) V. V. Demidov and M. D. Frank-Kamenetskii, *Trends Biochem. Sci.*, 2004, **29**, 62–71; (*b*) J. SantaLucia Jr. and D. Hicks, *Annu. Rev. Biophys. Biomol. Struct.*, 2004, **33**, 415–440.

9 (*a*) D. W. Wegman, F. Ghasemi, A. S. Stasheuski, A. Khorshidi, B. B. Yang, S. K. Liu, G. M. Yousef and S. N. Krylov, *Anal. Chem.*, 2016, **88**, 2472–2477; (*b*) H. Urakawa, S. El Fantroussi, H. Smidt, J. C. Smoot, E. H. Tribou, J. J. Kelly, P. A. Noble and D. A. Stahl, *Appl. Environ. Microbiol.*, 2003, **69**, 2848–2856.

10 (*a*) M. Olivier, *Mutat Res.*, 2005, **573**, 103–110; (*b*) A. P. Drabovich and S. N. Krylov, *Anal. Chem.*, 2006, **78**, 2035–2038; (*c*) Y. V. Gerasimova and D. M. Kolpashchikov, *Chem. Soc. Rev.*, 2014, **43**, 6405–6438; (*d*) M. Strerath, I. Detmer, J. Gaster and A. Marx, *Methods Mol. Biol.*, 2007, **402**, 317–328.

11 (*a*) D. M. Kolpashchikov, *J. Am. Chem. Soc.*, 2006, **128**, 10625–10628; (*b*) Y. V. Gerasimova and D. M. Kolpashchikov, *Biosens. Bioelectron.*, 2013, **41**, 386–390; (*c*) Y. V. Gerasimova, J. Ballantyne and D. M. Kolpashchikov, *Methods Mol. Biol.*, 2013, **1039**, 69–80; (*d*) M. Stancescu, T. A. Fedotova, J. Hooyberghs, A. Balaeff and D. M. Kolpashchikov, *J. Am. Chem. Soc.*, 2016, **138**, 13465–13468.

12 J. Feld and K. L. Carper, *Construction Failure Td Ed.*, John Wiley & Sons, 1997, ISBN: 0-471-57477-5.

13 P. Rice and H. Dutton, *Structural Glass*, Taylor & Francis, 1995, p. 33.

14 (*a*) M. R. Jones, N. C. Seeman and C. A. Mirkin, *Science*, 2015, **347**, 1260901; (*b*) L. Jaeger and A. Chworos, *Curr. Opin. Struct. Biol.*, 2006, **16**, 531–543; (*c*) Y. H. Roh, R. C. Ruiz, S. Peng, J. B. Lee and D. Luo, *Chem. Soc. Rev.*, 2011, **40**, 5730–5744; (*d*) M. Endo and H. Sugiyama, *ChemBioChem*, 2009, **10**, 2420–2443.

15 Y. V. Gerasimova, A. Hayson, J. Ballantyne and D. M. Kolpashchikov, *ChemBioChem*, 2010, **11**, 1762–1768.

16 (*a*) T.-J. Fu and N. C. Seeman, *Biochemistry*, 1993, **32**, 3211–3220; (*b*) B. F. Eichman, J. M. Vargason, H. M. M. Blaine and P. S. Ho, *Proc. Natl. Acad. Sci. U. S. A.*, 2000, **97**, 3971–3976; (*c*) D. M. Kolpashchikov, Y. V. Gerasimova and M. S. Khan, *ChemBioChem*, 2011, **12**, 2564–2567; (*d*) É. Boulais, N. P. D. Sawaya, R. Veneziano, A. Andreoni, J. L. Banal, T. Kondo, S. Mandal, S. Lin, G. S. Schlau-Cohen, N. W. Woodbury, H. Yan, A. Aspuru-Guzik and M. Bathe, *Nat. Mater.*, 2018, **17**, 159–166; (*e*) J. M. Stewart, H. K. K. Subramanian and E. Franco, *Nucleic Acids Res.*, 2017, **45**, 5449–5457; (*f*) J. M. Stewart, M. Viard, H. K. Subramanian, B. K. Roark, K. A. Afonin and E. Franco, *Nanoscale*, 2016, **8**, 17542–17550; (*g*) K. L. Lau and H. F. Sleiman, *ACS Nano*, 2016, **10**, 6542–6551; (*h*) J. Son, J. Lee, A. Tandon, B. Kim, S. Yoo, C. W. Lee and S. H. Park, *Nanoscale*, 2015, **7.**, 6492–6497.

17 K. Mdluli, R. A. Slayden, Y. Zhu, S. Ramaswamy, X. Pan, D. Mead, D. D. Crane, J. M. Musser and C. E. Barry, *Science*, 1998, **280**, 1607–1610.

18 H. T. Allawi and J. SantaLucia Jr., *Biochemistry*, 1997, **36**, 10581–10594.

19 (*a*) I. A. Pyshnaya, D. V. Pyshnyi, A. A. Lomzov, V. F. Zarytova and E. M. Ivanova, *Nucleosides, Nucleotides Nucleic Acids*, 2004, **23**, 1065–1071; (*b*) D. V. Pyshnyi,

A. A. Lomzov, I. A. Pyshnaya and E. M. Ivanova, *J. Biomol. Struct. Dyn.*, 2006, **23**, 567–580.

20 (*a*) S. Wang, A. E. Friedman and E. T. Kool, *Biochemistry*, 1995, **34**, 9774–9784; (*b*) H. Dai, M. Meyer, S. Stepaniants, M. Ziman and R. Stoughton, *Nucleic Acids Res.*, 2002, **30**, e86; (*c*) J. Hooyberghs, M. Baiesi, A. Ferrantini and E. Car-lon, *Phys. Rev. E: Stat., Nonlinear, Soft Matter Phys.*, 2010, **81**, 012901; (*d*) B. Rauzan, E. McMichael, R. Cave, L. R. Sevcik, K. Ostrosky, E. Whitman, R. Stegemann, A. L. Sinclair, M. J. Serra and A. A. Deckert, *Biochemistry*, 2013, **52**, 765–772.

21 D. Wu, Y. Zhou, H. Pan, P. Qu and J. Zhou, *Mol. Med. Rep.*, 2015, **11**, 1469–1475.